Silica-coated magnetic Fe_3O_4 nanoparticles as efficient nano-adsorbents for theimprovement of the vapor-phase adsorption of benzene

Mrs. T.PRASANTHI, Mr . P.RAVI PRAKASH

Mr. K.SREERAMULU (Corresponding Author)
GAYATRI COLLEGE OF SCIENCE & MANAGEMENT Accredited with by NAAC & ISO
(Affiliated to Dr. B R AMBEDKAR UNIVERSITY)
Under the Management of GURAJADA EDUCATIONAL SOCIETY
Munasabpeta, SRIKAKULAM – 532 401

ABSTRACT

In order to enhance benzene vapor-phase adsorption, this research concentrated on the fabrication of silica-coated Fe3O4 (Fe3O4@SiO2). Co-precipitation was used to make Fe3O4@SiO2, and FT-IR, SEM, and BET surface area measurements were used to characterize it. Using response surface approach, the optimal experimental conditions for benzene vapor-phase adsorption were determined (RSM). The optimal parameters for adsorption of vapor-phase benzene by Fe3O4@SiO2 were a residence period of 39.93 min, an initial benzene concentration of 13.57 mg l-1, and a temperature of 26.87°C. The experimental results were successfully matched to the Dubinin-Radushkevich (D-R) model, providing insight into the vapor-phase adsorption process of benzene on the Fe3O4@SiO2. By looking at the kinetics, such as the pseudo first-order (PFO) model and the pseudo second-order (PSO) model, the adsorption kinetics of benzene on Fe3O4@SiO2 could be better understood, and the experimental findings were shown to be in accordance with the PSO model. Based on the results of this research, magnetic Fe3O4@SiO2 is a promising low-cost nano-adsorbent.

Keywords: Benzene vapor-phase adsorption on magnetic Fe3O4@SiO2 nanoparticles using response surface technique.

INTRODUCTION

Among the many useful volatile organic compounds (VOCs), benzene is a crucial component of the chemical processing industry. There are a number of negative consequences associated with breathing in VOCs, including allergic responses, nausea, throat irritation, nasal irritation, eye irritation, and headaches. In addition, they contribute to major environmental issues such photochemical smog, air pollution, the loss of the ozone layer in the stratosphere, and rising global temperatures.

As a result, even trace amounts of VOCs may cause significant damage to the environment. During oil refining, petrochemical manufacture, and oil storage procedures, this harmful substance (benzene) is released from automobile exhaust or fuels that evaporate from tanks, vehicle carburetors, and petrol stations. 1-4 Emissions of air pollutants from the tailpipe are often correlated with the kind and quantity of gasoline used. Emissions from commonplace items and construction supplies including cement, drywall, paint, and adhesives also have a role. Another source of this contaminant is cigarette smoke. 5 The airflow of gases is significantly impacted by industrial processes. There is a negative impact on health due to the air quality decline. Reduce emissions of harmful gases into the atmosphere, and create mitigation plans, is essential. De-polluting techniques, therefore, are required. When compared to more conventional methods, nanotechnology offers superior solutions in the realm of adsorption technology. 6-7 Magnetic nanomaterials having unusual features like paramagnetism or ferromagnetism have received a lot of research interest in adsorption technology. In the realm of nanotechnology, magnetite (Fe3O4) is a common substance that has been studied extensively. 8 Due to its magnetic features, which include biocompatibility, low-toxicity, cheap cost, and large surface area, it has garnered a lot of interest. The addition of functional groups to Fe3O4 nanoparticles serves two purposes: (9) it decreases agglomeration and (10) it creates more adsorption active sites. 10-11 The magnetic property of Fe3O4, one of several magnetic compounds, aids recovery during the separation procedures. Fe3O4 nanoparticles have a highly developed pore structure in their pore volume, leading to an abundance of active sites. Agglomeration reduces pore capacity in metabolic hotspots. Particle agglomeration may be avoided by the use of coatings made of organic or inorganic surfactants. 12 Crystalline silica (SiO2) has unique chemical and physical features that make it a promising candidate for use in compounds made of inorganic materials used as surfactants. such as pseudo first-order (PFO) model and pseudo second-order (PSO) model.

1. MATERIALS AND METHODS

1.1. Materials

Chemicals such as tetraethyl orthosilicate (TEOS, Si(OC2H5)4), benzene (C6H6), iron (II) chloride

tetrahydrate (FeCl2.4H20), ethanol (CH3CH2OH), iron (III) chloride hexahydrate (FeCl3.6H2O), and ammonia SIGMA- The research used only substances and solvents

1.2. Preparation of the Fe_3O_4@SiO_2 magneticnanoparticles

During the production of Fe3O4, Fe (III) and Fe (IV) were both precipitated at the same time (II). The stoichiometric ratio of Fe+2/Fe+3 in a salt combination of FeCl2.4H2O and FeCl3.6H2O was 1/2, and the mixture was incubated in 50 mL of deionized water at 80 °C in the presence of argon gas for 30 minutes. The solution became a brilliant orange as soon as it was mixed together. Co-precipitation formed when 10 ml of NH3 solution was added gradually. In a flash, the color of the bulk solution changed from orange to black. For a further half hour, the amalgamation process was maintained with the help of argon. After five washes in a solution of ethanol and deionized water, the final result, Fe3O4, was clean and pure. The Fe3O4 was completely dry after being dried in a vacuum oven at 60 degrees Celsius for 24 hours. A shaker and a flask were used to combine 0.5 g of Fe3O4, 5 ml of ammonia, and 100 ml of ethanol. For 30 minutes, the mixed solution was ultrasonically agitated to provide a uniform texture. The mixture was then maintained at a high intensity while 0.4 ml of TEOS was added to the solution drop by drop. During the amalgamation, which took place in an argon gas environment, the temperature was kept constant at room temperature for a complete 12 hours. The Fe3O4@SiO2 product was magnetically separated and washed with deionized water and ethanol five times to eliminate any leftover contaminants. Fe3O4@SiO2 was dried for 24 hours in a vacuum oven at 60 degrees Celsius. Thirteen diagrams were used to illustrate the steps required to make Fe O @SiO.

As part of this study, silica-coated Fe3O4 (Fe3O4@SiO2) magnetic nanoparticles were created and used to improve benzene vapor-phase adsorption. Fe3O4@SiO2 was synthesized through co-precipitation and characterized using FT-IR, SEM, and BET surface area measurements. The experimental parameters for benzene vapor-phase adsorption were calculated using a Box-Behnken design (BBD) and a response surface methodology (RSM). The vapor-phase adsorption of benzene onto Fe3O4@SiO2 was investigated by examining a number of adsorption isotherms, including the Dubinin-Radushkevich (D-R), Freundlich, and Langmuir isotherms. Kinetics investigations elucidated the adsorption kinetics of benzene vapor on Fe3O4@SiO2..

Figure 1.

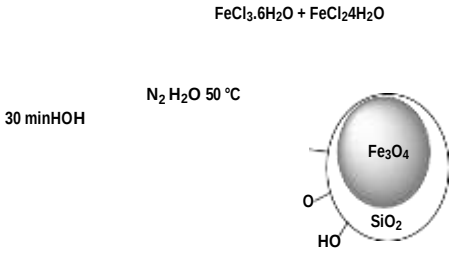

(NH3) were obtained from MERCK, ALFA AESAR,

of analytical purity in its procedures.

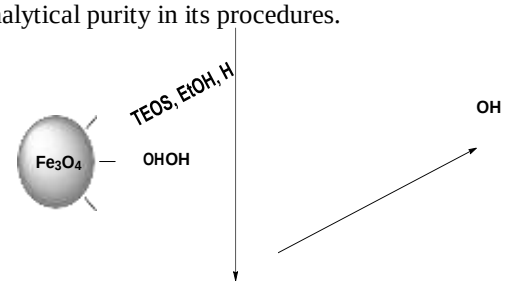

Figure 1. Schematic representation of the preparation of the Fe_3O_4@SiO_2 magnetic nanoparticles

1.3. Removal of benzene vapor by adsorption process

Previous work outlined the adsorption technique used in the benzene vapor removal utilizing Fe3O4@SiO2 magnetic nanoparticles. 14 For benzene vapor removal, we settled on a nitrogen (N2) flow rate of 100 ml min-1. For effective benzene vapor removal, the optimal dose of Fe3O4@SiO2 was 0.09 g. Benzene vapor adsorption capacity (in milligrams per gram) was defined as follows:15

Use of Design Expert 12.0.8.0 Software for Data Collection (Free Trial Version).

In this equation, m represents the optimal amount of Fe3O4@SiO2 to be used (in grams), F represents the flow rate (in liters per minute), Cin and Ceff represent the input and final benzene vapor concentrations (in milligrams per liter), and t represents the residence period (min).

2.4. Characterization

Spectra were acquired by Bruker-Vertex 70v Fourier Transform Infrared Spectroscopy. Pictures were captured using a ZEISS-EVO 50 scanning electron microscope. The Quantachrome-Nova equipment was used to calculate the Brunauer-Emmett-Teller (BET) surface area. Experiment-based mathematical modeling

SEM analysis

2. RESULTS AND DISCUSSION

2.1. Characterization of the Fe_3O_4@SiO_2 magnetic nanoparticles

The magnetic Fe3O4@SiO2 nanoparticles were characterized using scanning electron microscopy, Fourier transform infrared spectroscopy, and BET surface area. Figures 2, 3, and 4 show SEM images, FTIR spectra, and N2 gas adsorption/desorption isotherms, respectively, of these nanoparticles.

$q = F \int t(C - C$
) (1) respectively.

Surface morphology of magnetic nanoparticles made of Fe3O4 and Fe3O4@SiO2 was analyzed using SEM. Micrographs of Fe3O4 and Fe3O4@SiO2 taken by a scanning electron microscope (scale length = 500 nm) were shown in Figure 2. It was known that the rough surface of Fe3O4 contributed to its high dispersion. The pore structure was found to be rough and spongy. It was easy to see the pores and crevices on the surface of the Fe3O4@SiO2. It was realized that the surface area of the Fe3O4@SiO2 microstructure was enhanced by the intrusions, protrusions, and roughness. The sizes of the magnetic nanoparticle spheres are estimated to be between 70 and 110 nm, taking the length of the scale into account..[16]

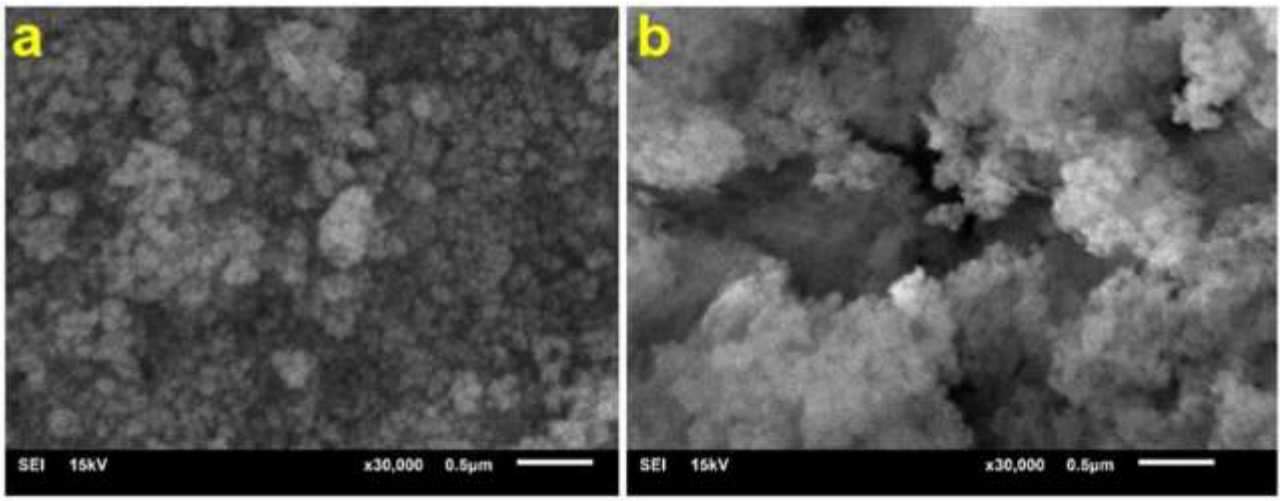

Figure 2. SEM images of the Fe_3O_4 (a) and Fe_3O_4@SiO_2 (b) magnetic nanoparticles.

2.1.1. FTIR analysis

Figure 3 shows the FTIR spectra of Fe3O4 and Fe3O4@SiO2 magnetic nanoparticles. The existence of Fe3O4 was confirmed by the FTIR spectra, which showed a distinctive absorption peak at 552 cm-1, corresponding to the Fe-O bond. Peaks of vibrational stretching, bending, and deformation were detected at 3446 cm-1, 1654 cm-1, and 1480 cm-1, respectively.

the water that was absorbed (-OH). The bending vibration of the Si-O bond, at 570 cm-1, and the stretching vibration of the Si-OH bond, at 964 cm-1, were newly detected peaks in the FTIR spectrum of the Fe3O4@SiO2. The stretching vibration of the asymmetric Si-O-Si bond contributed to the peak at 1082 cm-1. This signal demonstrated that SiO2 had effectively covered the Fe3O4 surface. When comparing the FTIR spectra of Fe3O4 and Fe3O4@SiO2, we found that they agreed with those reported in the literature. 17

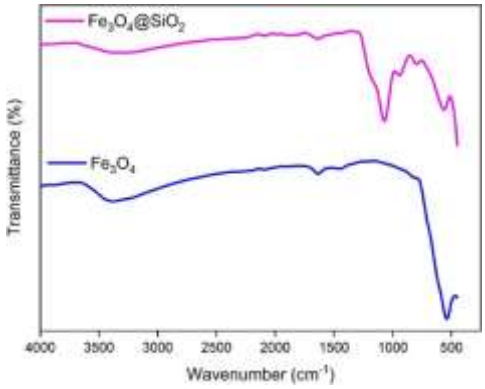

Figure 3. FT-IR spectrum of the Fe_3O_4 and Fe_3O_4@SiO_2 magnetic nanoparticles

2.1.2. BET analysis

Presented in Figure 4 are the adsorption and desorption

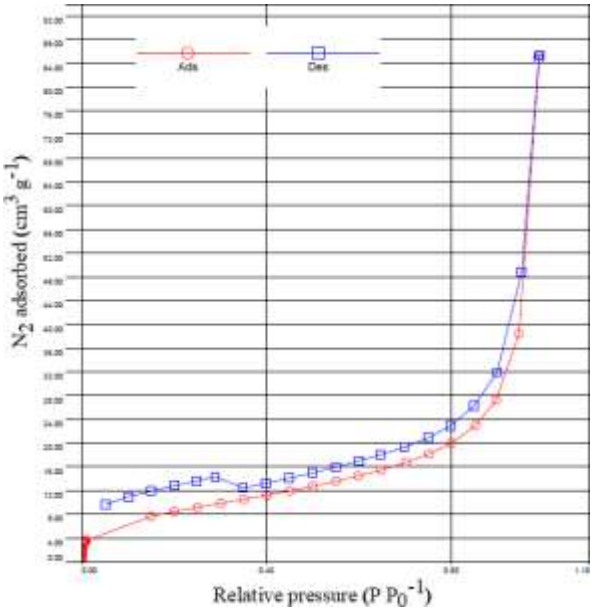

isotherms for magnetic Fe3O4@SiO2 nanoparticles, which have a BET surface area of 28.97 m2 g-1. Figure 4 analysis revealed that Fe3O4@SiO2 satisfied the IUPAC requirements for the H3 type hysteresis cycle and the IV type curve. Layers of homogenous mesopores were also predicted to exist. The SiO2 alteration had an effect on the surface area of Fe3O4@SiO2, as seen by the material's relatively low value. This occurred due to the presence of SiO2, which penetrated the surface and formed a shell around the magnetic nanoparticles.

Figure 4. N_2 adsorption and desorption isotherms of the Fe_3O_4@SiO_2 magnetic nanoparticles

3.2. Experimental design and optimization

Using RSM, an experimental method for optimizing the design process, the authors of the present study

explore how important it is to think about how the operational parameters could interact with one another. The RSM-based BBD technique was used to conduct statistical tests and generate the resultant regression model. An evaluation of all available statistical analyses for modeling and improving experimental studies on benzene vapor-phase adsorption was conducted. The performance of the parameters and their interactions was analyzed using ANOVA and three-dimensional visualizations inside the program. To get the equation for the general quadratic model, an ANOVA test and the BBD technique were used to examine the association between the variables. The expected adsorption capacity values for a variety of parameter values were calculated using the derived quadratic model equation. The p-value, adeq precision, and F-value were analyzed to evaluate the program's correctness, and the obtained R2 was utilized to evaluate the importance of the model projected by the program. The study used a three-variable BBD to examine the cause-and-effect dynamic between inputs and outcomes. For this research, we zeroed emphasis on the effects of residence time, initial benzene concentration, and temperature on adsorption performance in the vapor phase. The adsorption capacity of vapor-phase benzene was considered as the answer. Three separate color-coded numbers represented the BBD's analytical parameters. The results from the BBD approach are shown in Table 1, while the results from the experimental design levels with independent components are presented in Table 2. Results from an investigation of statistical compatibility using ANOVA are shown in Table 3. The analysis of variance (ANOVA) results put the p-value of the recommended model at 0.0001, meaning that the model generated by the software can adequately define 99.99% of the outcomes seen in the lab conditions of the tests expected by the software. There was an excellent match between the experimental data and the expected model, as shown by the high values of R2 (99.89), F-value (>4), and adeq accuracy (>40%). 18-19 Table 2 also shows a good agreement between observed and expected adsorption capacities, providing more evidence for the validity of the predicted model.

Table 1. Experimental design levels with independent factors

Factors	Coded values		
	-1	0	+1
Residencetime (X_1) (min)	20	30	40
Concentration (X_2) (mg l^{-1})	10	12.5	15
Temperature (X_3) (°C)	25	30	35

Figure 5 presented three-dimensional (3D) plots achieved with the program, showing the influence of initial benzene concentration, adsorption temperature and residence time on the vapor-phase adsorption capacity of benzene. It could be observed in Figure 5a that the vapor- phase adsorption capacity of benzene increased with the increase in residence time.

Table 2. Experiment design results obtained for the vapor-phase adsorption of benzene by the $Fe_3O_4@SiO_2$ magnetic nanoparticles.

Run	Time (min)	Concentration (mg l^{-1})	Temperature (°C)	Actual adsorption capacity (mg g^{-1})	Predicted adsorption capacity (mg g^{-1})
1	30	12.5	30	80	83
2	20	15	30	50	57
3	20	10	30	41	40
4	30	15	35	60	58
5	40	12.5	35	150	162
6	30	12.5	30	80	86
7	20	12.5	25	45	53
8	40	15	30	185	190
9	40	10	30	160	157
10	30	12.5	30	82	85
11	30	15	25	110	116
12	40	12.5	25	198	201
13	30	10	25	70	68
14	30	12.5	30	80	89
15	30	10	35	55	57
16	20	12.5	35	36	28
17	30	12.5	30	80	85

Table 3. ANOVA results created in accordance with the BBD approach

Source	Sum of squares	df	F-value	p-value	
Model (quadratic)	20627.11	9	678.81	< 0.0001	Significant
X_1	8532.50	1	5005.50	< 0.0001	
X_2	8247.96	1	115.09	< 0.0001	
X_3	191.84	1	274.47	< 0.0001	
X_1X_2	1545.57	1	9.44	0.0180	
X_1X_3	0.0071	1	56.10	0.0001	
X_2X_3	3.64	1	45.18	0.0003	
X_1^2	1242.51	1	598.85	< 0.0001	
X_2^2	1181.88	1	3.73	0.0948	
X_3^2	472.13	1	10.96	0.0129	

R^2 = 0.9989, Adeq precision = 80.50

Adsorption equilibrium was reached within a short period on Fe3O4@SiO2 due to the low density of active sites. 20 Adsorption from the gas phase is shown to be hindered by temperature in Figure 5b. With rising temperatures, adsorption effectiveness decreased. The inactivation of active bond sites on the adsorbent may also contribute to a decrease in the adsorbed amount with rising temperature. 21 A surface plot of the initial benzene concentration against temperature is shown in Figure 5c, and it can be seen that this variable has no discernible effect on the vapor-phase adsorption capacity. There has been an increase in vapor-phase adsorption, as measured by,

mainly because benzene has lost interest in Fe3O4@SiO2. Similar trends have been seen in the past. 14, 22

Benzene vapor phase adsorption capacity of

Fe3O4@SiO2 was determined by adjusting the process conditions. Analytical calculations were made using the model equation for the predicted values from the quadratic model to determine the optimum circumstances. In this case, the ideal values were determined to be a residency duration of 39.93 minutes,

At the outset, the benzene content was 13.57 mg l-1, and the temperature was 26.87°C. It was determined that 197.50 mg g-1 of benzene could be adsorbed onto Fe3O4@SiO2 in the gas phase.

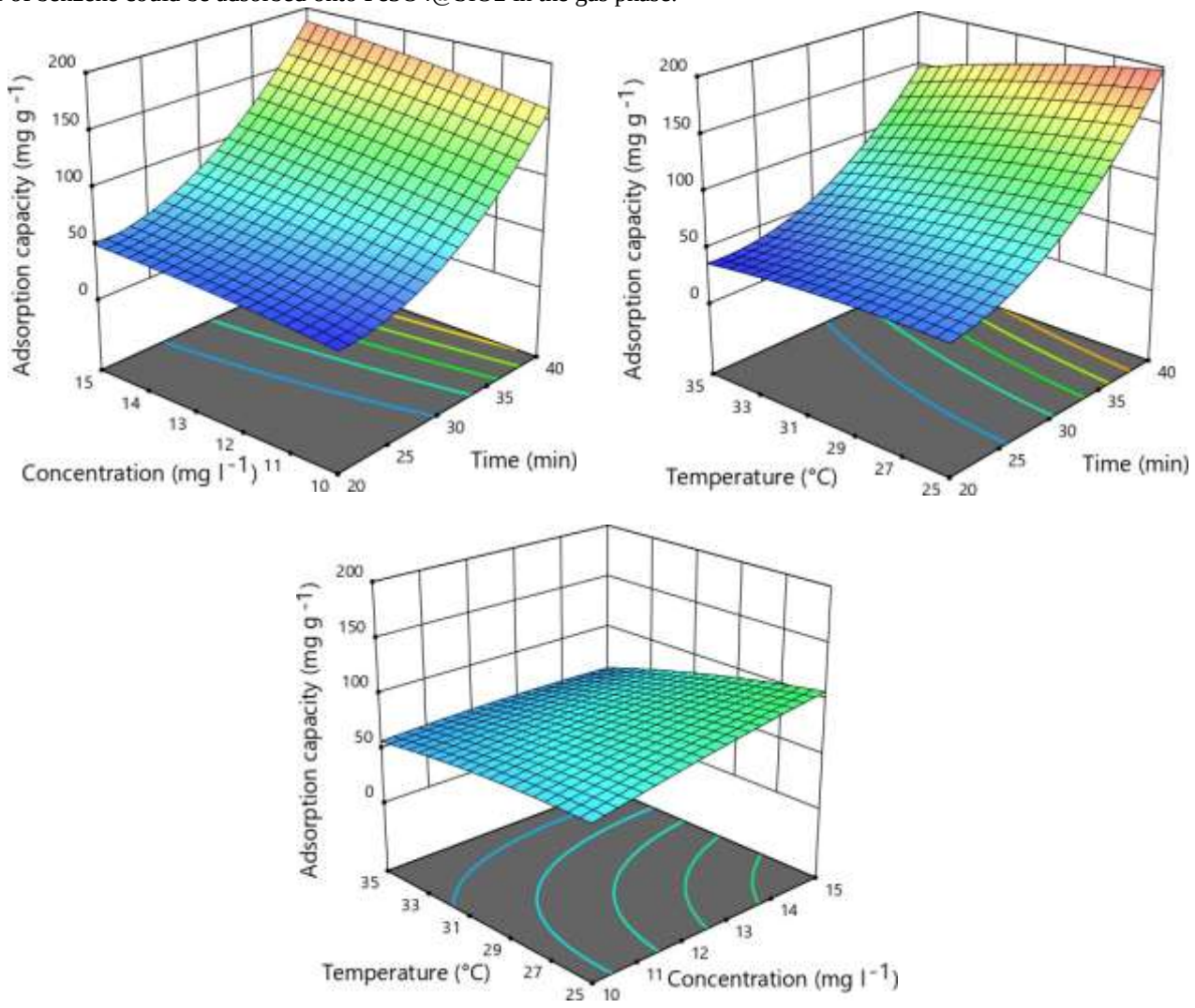

Figure 5. The influence of parameters on the vapor-phase adsorption capacity of benzene.

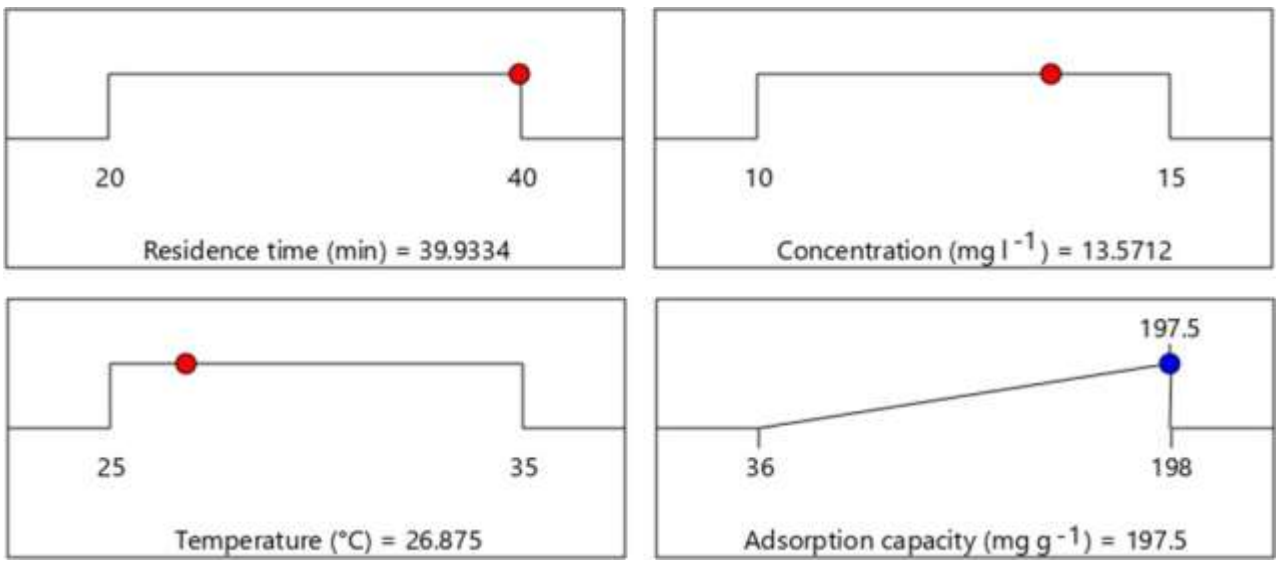

Figure 6. Optimum values for the vapor-phase adsorption of benzene

3.3. Kinetic studies

Researching kinetics such as the pseudo first-order (PFO) model and the pseudo second-order (PSO) model under ideal conditions created by RSM clarified the vapor-phase adsorption kinetics of benzene on the Fe3O4@SiO2. The PFO model states that the adsorption rate is proportional to the number of available site locations. 23 It was hypothesized under the PFO model that levels of focus would rise with time. The non-linear kinetic equation for the PFO model is given in Eq (2). The PSO model equation is based on the capacity of the adsorption equilibrium, which states that the number of active sites on the adsorbent's surface directly affects the adsorption rate. 23 The non-linear PSO model was described in Eq (3). 24

3.4. Isotherm studies

The vapor-phase adsorption mechanism of benzene on the Fe3O4@SiO2 was elucidated by analyzing the isotherms, namely the Dubinin-Radushkevich (D-R), Freundlich, and Langmuir isotherms, under the optimal conditions determined by RSM. For adsorption onto a single layer of a surface, where there may or may not be many copies of the layer, the Langmuir adsorption isotherm holds true. The model assumes that there is no adsorbate movement at the surface plane and that the adsorption energies on the surface are all the same. With these presumptions in mind, we may write out the Langmuir model as Eq (4). According to the Freundlich isotherm theory, there is a non-constant relationship between the quantity of solute adsorbed on a given sorbent mass and the solute concentration. Non-linear Freundlich equation

$q_t = (1 - e^{-kff\ t})$ (2)

In Eq., an isotherm model was provided (5). 25 To characterize the impact of the porous medium, the D-R isotherm model was created.

$q_t = \frac{q_e^2\ t}{1+k_s q_e}$ (3)

rate constant (mg g-1 min-1) (g mg-1 min-1).

sorbents' architectural layout. The theory is based on the idea of adsorption potential and the hypothesis that, in contrast to layered adsorption on pore walls, the adsorption process

The experimentally predicted PSO for benzene vapor-phase adsorption was followed by Fe3O4@SiO2.

Where qe and qt are the equilibrium and time t adsorption capacities (mg g-1), kf is the PFO model's rate constant (1 min-1), and ks is the PSO model's

is connected to the filling of the microporous space. 26-27 Non-linear form of this model first appeared in Eq (6). 28 Adsorption free energy, E in Eq. (6), is the average energy required to hold one particle in place.

Equation (E) demonstrated the value E. (8). 28 model (Figure7andTable4). (Figure7andTable4). $q_e = \frac{q_m\ C_e}{1+K_L C_e}$ (4)

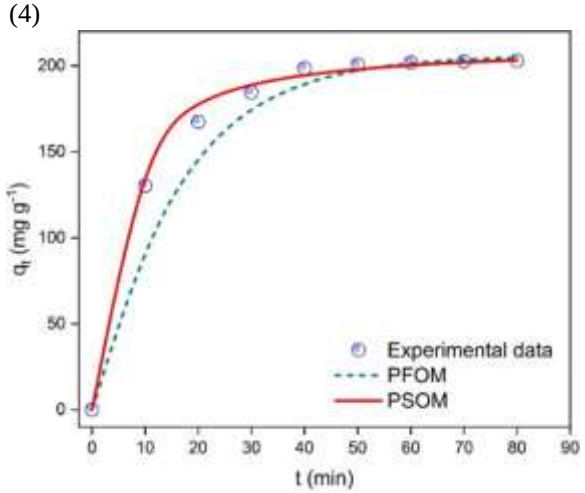

$q_e = K_F C_e^{\frac{1}{n}}$ (5)

$= q_m\ e(-\beta\varepsilon^2)$ (6)

$\varepsilon = RTln(1 +$

$E = \frac{1}{\sqrt{2\beta}}$

$\frac{1}{C_e}$

Figure 7. Adsorption kinetic models of benzene by theFe_3O_4@SiO_2 magnetic nanoparticles

Table 4. Adsorption kinetic parameters of benzene by the $Fe_3O_4@SiO_2$ magnetic nanoparticles

Kinetic models	Parameters	Values
PFO model	q_e	205.952
	k_f	0.0648
	R^2	0.967
PSO model	q_e	212.45
	k_s	0.0013
	R^2	0.990

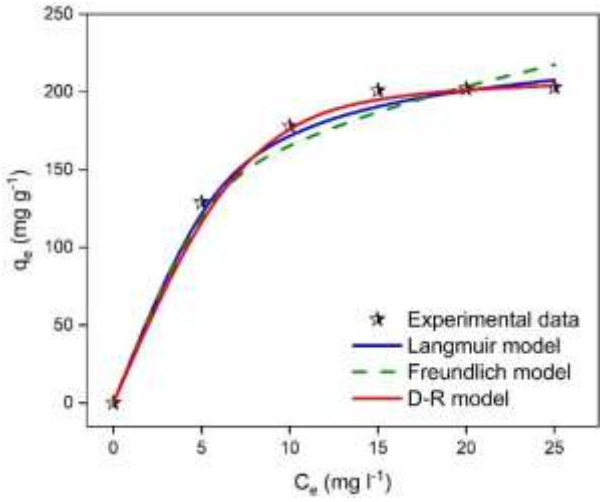

If n is between 1 and 10, indicating a suitable adsorption process, then qm is the maximum adsorption capacity (mg g-1), is the adsorption isotherm constant, and Ce is the equilibrium concentration of the adsorbate in milligrams per liter. The dominance of physical adsorption is at E 8 kJ mol-1. While ion exchange is responsible for adsorption when the energy barrier is 8 kJ mol1 to 16 kJ1 and diffusion when the energy barrier is 16 kJ mol1. 29

The research found that the Langmuir model gave an estimate of qmax of 237.192 mg g-1 and KL of 0.281 l mg-1. Calculating the R2

was 0.999, suggesting that the Fe3O4@SiO2 vapor-phase adsorption equilibrium isotherm data were better matched to the D-R model. The study's E value of 0.463 kJ mol-1 suggests that the adsorption of benzene in the vapor phase was a physical process (Figure 8 and Table 5). The n value of the Freundlich model was also determined to be 3.472, suggesting that benzene's vapor-phase adsorption process was a saturable one. suitable.[30]

Figure 8. Adsorption isotherm models of benzene by the $Fe_3O_4@SiO_2$ magnetic nanoparticles

Table 5. Adsorption isotherm parameters of benzene by the $Fe_3O_4@SiO_2$ magnetic nanoparticles

Isotherm models	Parameters	Values
Langmuir	q_{max}	237.192
	K_L	0.281
	R^2	0.997
Fruendlich	K_F	86.056
	n	3.472
	R^2	0.991
D-R	q_m	208.721
	β	$2.334*10^{-6}$
	E	0.463
	R^2	0.999

3. CONCLUSIONS

In order to enhance benzene vapor-phase adsorption, this work concentrated on the production of Fe3O4@SiO2. The co-precipitation technique was used to create the Fe3O4@SiO2, and FT-IR, SEM, and BET surface area studies were used to characterize it. Benzene adsorption capacity was measured in the vapor phase using BBD and RSM, and the experimental parameters were analyzed. Under ideal circumstances (39.93 min residence duration, 13.57 mg l-1 starting benzene concentration, and 26.87°C temperature), 197.50 mg g-1 of the vapor-phase benzene was adsorbed by the Fe3O4@SiO2 particle. By analyzing several isotherm models, including the Dubinin-Raduskevich (D-R), Freundlich, and Langmuir isotherms, we were able to better understand the vapor-phase adsorption process of benzene on Fe3O4@SiO2.

The D-R model provided a good match for the perinatal data. Investigating kinetics such as the PFO model and the PSO model elucidated the vapor-phase adsorption kinetics of benzene on the Fe3O4@SiO2, with experimental data conforming to the PSO model. The results of this research show that magnetic Fe3O4@SiO2 nano-adsorbents have great promise as low-cost vapor-phase adsorbents for benzene.

REFERENCES

1Ahin, S.; Horoz, S.; Kutluay, S.; Ece, M.; Ind. Eng. Chem. Res. 2020, 59 (48), 21106-21123.
Fuel 2021, 287, 119691 Kutluay, S.
Colloid Surf. A-Physicochem. Eng. Asp. 2021, 609, 125848 Kutluay, S., and Temel, F.

Environ. Sci. Pollut. Res. 2021, 28 (5), 5231-5253. 4. ahin,.; Kutluay, S.; Horoz, S.; Ece, M.
Environ. 5. Wallace, L. A. The Journal of Public Health, 1989;82(2):165-169.
J. Environ. Sci. 2018, 67, 104-114; Yang, X.; Yi, H.; Tang, X.; Zhao, S.; Yang, Z.; Ma, Y.; Feng, T.; Cui, X.
7 Wibowo N., L. Setyadhi, D. Wibowo, J. Setiawan, and S. Ismadji. 146 (1-2) 237-242 (2007), J. Hazard. Mater.
8. de las Nieves Chem. Eur. J. 2018, 24 (49), 12820-

12826. Pia, M., Rodriguez, P., Gutiérrez, M. S., Quionero, D., Morey, J., & Frontera, A.
J. Environ. Sci. 2015, 31, 164-174. 9. Connie, Z. Y., and Ariya, P. A.
Roto R, Yusran Y, Kuncaka A. Appl. Surface Science 377 (2016), 30-36.
Environ. Dev. Sustain. 2017, 11 Mohamed, E. F. (2).
12. Duan, S.; Xu, X.; Liu, X.; Wang, Y.; Hayat, T.; Alsaedi, A.; Meng, Y.; Li, J. J. Colloid Interface Sci. 2018, 513, 92-103.
13. Zandipak, R.; Sobhan Ardakani, S.; Shirzadi, A. Sep. Sci. Technol. 2020, 55 (3), 456-470.
J. Environ. Chem. Eng. 2019, 7 (2), 102947. 14 Kutluay, S.; Baytar, O.; ahin,.
Chem. Eng. J. 2015, 259, 7989; Zhao, Z.; Wang, S.; Yang, Y.; Li, X.; Li, J.; Li, Z.
J. Nanobiotech. 2020;18(1):155; Ma, C.; Li, C.; He, N.; Wang, F.; Ma, N.; Zhang, L.; Lu, Z.; Ali, Z.; Xi, Z.; Li, X. J. Biomed. Nanotechnol. 2012;8(6):1000-1005.
18 Kutluay S., Ece M., and Sahin S., International Journal of Chemical Technology 2020, Volume 4, Issue 2, Pages 146–155.
New J. Chem., 2020, 44 (30), 12949-12961; Temel, F., and Kutluay, S.
20. Vohra, M. S. Arab. J. Sci. Eng. 2015, 40 (11), 3007- \s3017.
Bioresour. Technol. 2008, 99(8), 3100-3109; Padmavathy, V.
22. Kutluay, S.; Baytar, O.; Şahin, Ö. Res. Eng. Struct. Mater. 2019, 5 (3), 279-298.

Ecol. Eng. 2016, 91, 317-332. Ali RM, Hamad HA, Hussein MM, and Malash GF.
24. Vora, S.; Khimani, M.; De, C. Ecol. Eng. 2013, 34 \s(7), 947-956.
Reference number 25: Salih WM, Gzar HA, Hassan NF, J. Eng. 2012, 18 (9), 1042-1054.
Sep. Purif. Technol. 2020, 116681 (Laskar, I. I., and Z. Hashisho).
J. Nanomater. 2016, Abbas A., Abussaud B. A., Al-Baghli N. A., Khraisheh M., and Atieh M. A.
2019;277:646-648 J. Mol. Liq.
RSC Adv. 2016, 6 (72), 67630-67642; Sadeghalvad, B.; Azadmehr, A.; Hezarkhani, A.
30. Wang, C.; Zhong, H.; Wu, W.; Pan, C.; Wei, X.; Zhou, G.; Yang, F. ACS Omega 2019, 4 (1), 1652-1661.